Absolute measurement of radiative and Auger rates of K-shell-vacancy states in highly charged Fe ions

R. Steinbrügge,[1,*] S. Bernitt,[1] S. W. Epp,[2] J. K. Rudolph,[1,3] C. Beilmann,[1,4] H. Bekker,[1] S. Eberle,[1] A. Müller,[3] O. O. Versolato,[1] H.-C. Wille,[5] H. Yavaş,[5] J. Ullrich,[1,†] and J. R. Crespo López-Urrutia[1]

[1]*Max-Planck-Institut für Kernphysik, Saupfercheckweg 1, 69117 Heidelberg, Germany*

[2]*Max Planck Advanced Study Group, CFEL, Notkestraße 85, 22607 Hamburg, Germany*

[3]*Institut für Atom- und Molekülphysik, Justus-Liebig-Universität Gießen, Leihgesterner Weg 217, 35392 Gießen, Germany*

[4]*Physikalisches Institut, Ruprecht-Karls-Universität Heidelberg, Im Neuenheimer Feld 226, 69120 Heidelberg, Germany*

[5]*Deutsches Elektronen-Synchrotron (PETRA III), Notkestraße 85, 22607 Hamburg, Germany*

(Received 21 October 2014; published 3 March 2015)

We present absolute measurements of radiative and Auger decay rates of K-shell vacancies in highly charged iron ions. The ions were resonantly excited with monochromatic x rays from the PETRA III synchrotron source. By measuring x-ray fluorescence and Auger decay simultaneously, absolute transition rates could be determined independently of most experimental parameters. The results confirm theoretical calculations, which are essential to model the photoexcited plasmas in x-ray binary stars and active galactic nuclei.

DOI: 10.1103/PhysRevA.91.032502 PACS number(s): 32.70.Fw, 32.80.Fb, 95.30.Dr

I. INTRODUCTION

The $K\alpha$ lines of highly charged iron ions are among the most prominent features in the x-ray spectra of laboratory and astrophysical plasmas. Due to their high transition rates and the relatively large abundance of iron, they have been observed in a plethora of celestial sources. They provide insight into the dynamics of accretion disks of x-ray binaries [1–3] and active galactic nuclei [4–10] and have been used recently to discover highly charged irons in relativistic jets [11]. Often x-ray observatories cannot resolve single lines or different charge states. Only a few observations show hints of $K\alpha$ transitions in charge states other than Fe XXVI or Fe XXV [12–14], which were seen in solar flares [15]. As these transitions contribute to the intensity and width of the unresolved $K\alpha$ line, they are necessary constituents of spectral modeling. For iron ions with a K-shell vacancy, the Auger decay rates are of the same order as the radiative rates, thus knowledge of the fluorescence yield is important for the determination of ion abundances. Therefore, many theoretical calculations of transition energies and decay rates have been performed (see Refs. [16–20] and references therein). Laboratory measurements were performed with plasmas produced in tokamaks [21,22] and electron beam ion traps (EBITs) [23]. The emission line energies were measured with high precision using Bragg crystal spectrometers, but determining absolute decay rates was not possible because of the complexity of the excitation processes, namely, electron-impact ionization, inner-shell ionization, or dielectronic recombination (DR). Only one measurement reported absolute dielectronic recombination resonance strengths, by comparing DR intensities to those of radiative recombination [24]. With the advent of ultrabrilliant x-ray sources, recently it became possible to excite the transitions radiatively, allowing one to measure their natural linewidths [25].

Studies of the photoionization of ions have been traditionally carried out using so-called merged-beam methods [26], where an ion beam is superimposed onto a photon beam from a suitable source, in general, a synchrotron. By this method, K-shell photoionization has been measured for several low charge states of light ions, as listed in Table I. However, the achievable ion-beam densities limit the application of these methods for higher charge states. The use of ions trapped in an EBIT as a target allows one to investigate these charge states, as demonstrated for Ar^{8+} [27] and Fe^{14+} [28].

II. EXPERIMENTAL METHOD

Here we present an extension of this technique, in which a simultaneous fluorescence measurement allows the determination of Auger and radiative decay rates for several excited states in Li-, Be-, and C-like iron ions (see Fig. 2). This was achieved by combining the natural linewidth measurements of Rudolph *et al.* [25] with a photoion detection system to determine the relative branching ratio between radiative and Auger decay. Together with a measurement of the relative oscillator strength of the fluorescence, this allows us to obtain absolute values for the decay rates. We employ the now well-established combination of the transportable FLASH-EBIT with an intense x-ray source [25,27–31] and monitor the charge-state distribution to detect photoionization.

The experimental setup is shown in Fig. 1. An electron beam emitted by a cathode is accelerated towards the trap center, where it is compressed to 50 μm by a 6-T magnetic field and afterwards dumped on a cylindrical collector. The injected atoms are ionized by electron-impact ionization and radially trapped by the space charge of the electron beam. Axial trapping is achieved via an electrostatic potential well created by drift tubes along the beam. Lowering the collector side of this well enables the ions to escape from the trap through the collector. They are then 90° deflected by an energy-selective electrostatic bender and guided to a velocity filter. There the ions are separated by their charge-to-mass ratio and afterwards recorded on a position-sensitive detector. The ion cloud in the trap is illuminated with x rays from the

*rene.steinbruegge@mpi-hd.mpg.de

†Present address: Physikalisch Technische Bundesanstalt (PTB), Bundesallee 100, 38116 Braunschweig, Germany.

TABLE I. List of K-shell photoionization measurements performed in merged-beam experiments. For a comparison with the presented experiment, the accuracy of the measured linewidth is given, which in these low-Z systems is solely determined by the Auger decay rate.

Ion	Resonance energy (eV)	Accuracy $\Delta\Gamma/\Gamma$	Reference
Li^{+}	150	5%	[32]
B^{+}	194	4%	[33]
B^{2+}	199	8%	[34]
C^{2+}	294	18%	[35]
C^{3+}	303	19%	[36]
N^{+}	401	12%	[37]
N^{2+}	405	52%	[38]
N^{3+}	414	14%	[39]
N^{4+}	421	72%	[39]
Fe^{23+}	6653	7%	This experiment

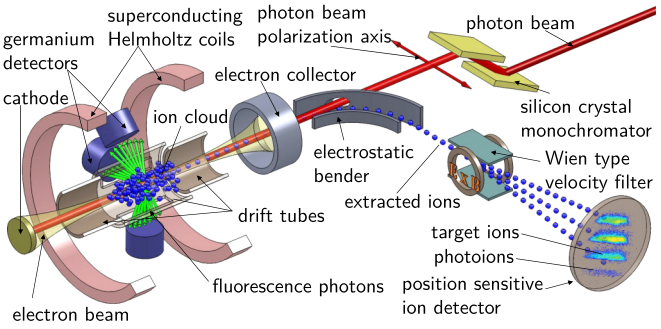

FIG. 1. (Color online) Scheme of the experimental setup. An electron beam accelerated toward the trap center and compressed by a coaxial 6-T magnetic field produces highly charged iron ions. The ions are continuously extracted from the trap and guided through a velocity filter, which separates the different charge states, to a position-sensitive detector. A monochromatic x-ray beam resonantly excites the ion cloud in the trap and fluorescence is registered by germanium photon detectors.

PETRA III synchrotron. At the Dynamics beamline P01 two 5-m undulators produce a high-flux linearly polarized photon beam, which is monochromized with a double-crystal high heat load monochromator (HHLM) [40]. The resolution of the HHLM can reach 300 meV full width at half maximum at 6.6 keV, which allows one to selectively excite single K-shell transitions in the trapped ions. The Auger decay of an excited ion corresponds to resonant photoionization, so it was detected by the increased charge state of the photoion. To minimize the background due to electron-impact ionization, the electron-beam energy of the EBIT was set to a value below the ionization threshold of the investigated ion. Simultaneously to the photoions, fluorescence photons are detected by three germanium detectors mounted at angles of 0°, 45°, and 90° with respect to the polarization of the photon beam.

III. MEASUREMENTS AND DATA ANALYSIS

With this setup we excited and measured various K-shell transitions of highly charged iron ions, as shown in Fig. 2. An overview of the detected fluorescence and photoionization spectra is shown in Fig. 3. The photoion count rates are much lower than the fluorescence rates because technical reasons limited the efficiency of the process of extracting, charge separating, and detecting the photoions. Therefore we did not analyze the photoionization data with respect to transition energies, as they can be determined more accurately with the fluorescence signal [25]. For the transitions q and u no photoionization was detected, because they do not have significant Auger decay channels.

Our measurement scheme for absolute decay-rate determination employs taking data of at least two transitions for each charge state and comparing them to suppress setup-dependent uncertainties. These transitions are r, q, t for Li-like, $E1$, $E2$ for Be-like, and $C1$, $C2$ for C-like iron (see Fig. 2), or indexed 1,2 when no specific charge state is considered. Besides the total radiative (A_γ) and total Auger rates (A_A), the measured yields (Y) also depend on the number of ions in the trap (N_{ion}), the total photon flux (N_γ), the excitation cross section (σ), and the detection efficiency of the ion extraction beamline (P_{ion})

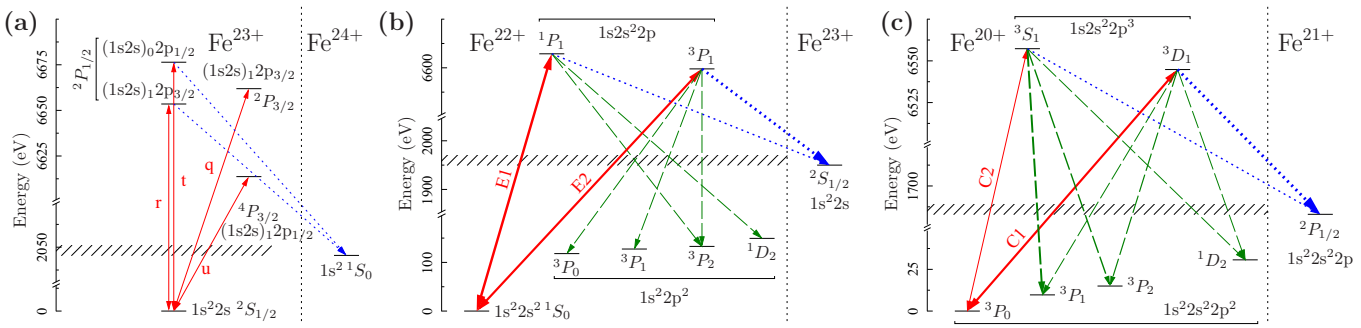

FIG. 2. (Color online) Grotrian diagrams of the measured iron ions: (a) Li-like, (b) Be-like, (c) C-like. Only levels with importance to the measurement are shown. The red (solid) transitions are directly excited by the PETRA III photon beam. Radiative transitions to other states are green (dashed), and the blue (dotted) transitions are Auger decays. In (b) and (c) the thickness of the arrows indicates the relative probabilities for a decay to that level, taken from Ref. [17]. For simplicity, only the main Auger decay channel is shown, as the measurement does not distinguish different Auger channels.

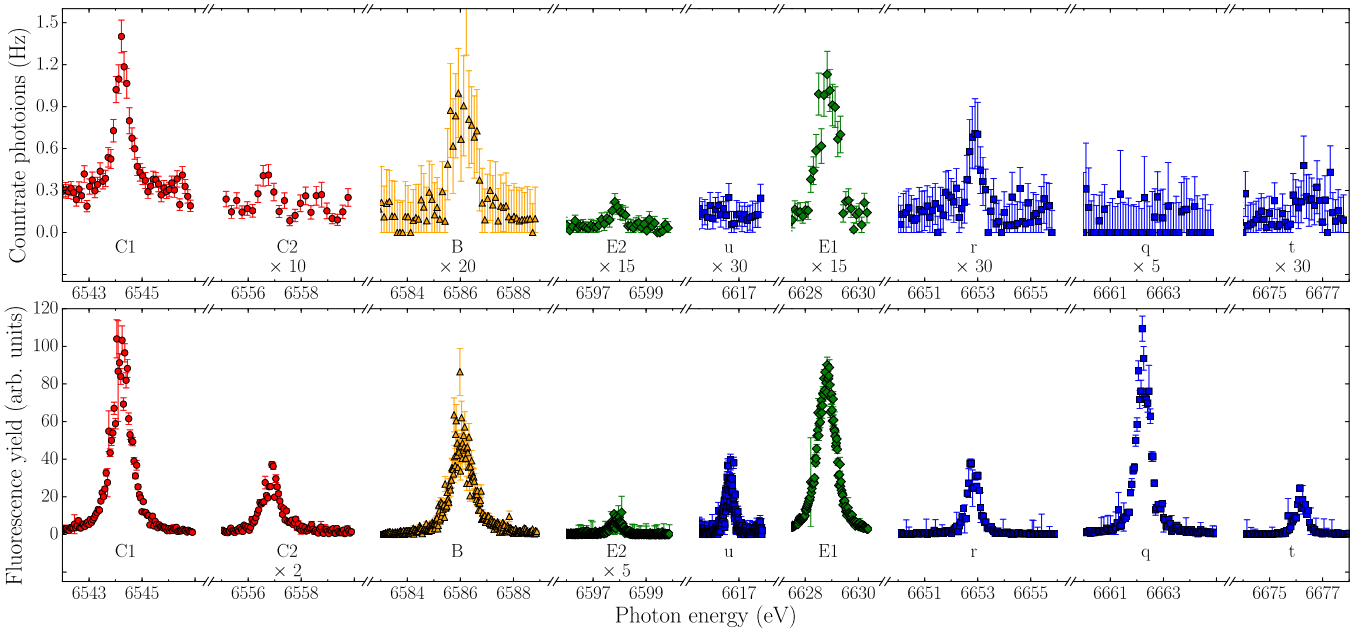

FIG. 3. (Color online) Overview of the measurement results of the scans for the different iron charge states. The top panel shows the ion yields of the photoions, while the fluorescence photon yield is plotted in the bottom panel. The colors represent different measurements for C-like (red circles), B-like (yellow triangles), Be-like (green diamonds), and Li-like (blue squares) iron. Note that most data are scaled up by a factor indicated below the line label. The intensities of the fluorescence yield are comparable only within each charge state.

and the germanium detectors (P_γ):

$$Y_{\text{ion}} = \frac{A_{\text{A}}}{A_\gamma + A_{\text{A}}} \sigma N_{\text{ion}} N_\gamma P_{\text{ion}}, \tag{1}$$

$$Y_\gamma = \frac{A_\gamma}{A_\gamma + A_{\text{A}}} \sigma N_{\text{ion}} N_\gamma P_\gamma. \tag{2}$$

As the ion and photon yield are measured at the same time, their ratio is independent of cross section, ion number, photon flux, and photon energy. We measured this ratio for the two transitions. As only the photon beam energy is changed, the detection efficiencies are essentially the same for both measurements. This allows one to calculate the ratio of branching ratios (called parameter c in the following), which solely depends on the transition rates:

$$c := \frac{Y_{\gamma,1}/Y_{\text{ion},1}}{Y_{\gamma,2}/Y_{\text{ion},2}} = \frac{A_{\gamma,1}}{A_{\text{A},1}} \frac{A_{\text{A},2}}{A_{\gamma,2}}. \tag{3}$$

To maximize the ion yield, the measurements of this parameter were carried out with the photon beam energy fixed at the resonance maximum.

In a second set of measurements, we scanned the energy of the photon beam by stepwise changing the angle of the monochromator crystal. Parts of this data set are common to Ref. [25]. To minimize the systematic errors, we choose the scan range so that at least two resonances of a charge state are covered. For further analysis we only use the fluorescence data, as their count rates are higher than the rates of detected ions. By fitting the obtained resonances to a Voigt profile, we obtain the area S_γ of the peaks. This area is proportional to the line strength S of the transition,

$$S_\gamma = \int Y_\gamma dE \propto \frac{A_\gamma}{A_\gamma + A_{\text{A}}} S. \tag{4}$$

The line strength S is proportional to $g\frac{A_\gamma}{\nu^2}$, where g is the degeneracy of the excited state and ν the photon frequency of the resonance, which was measured precisely in Ref. [25]. In the ratio of the areas of the two transitions (parameter d in the following), the proportionality constants cancel, and we get a value only depending on the transition rates,

$$d := \frac{S_{\gamma,1}}{S_{\gamma,2}} = \frac{A_{\gamma,1}^2}{A_{\gamma,2}^2} \frac{(A_{\gamma,2} + A_{\text{A},2})}{(A_{\gamma,1} + A_{\text{A},1})} \frac{\nu_2^2}{\nu_1^2} \frac{g_1}{g_2}. \tag{5}$$

The parameters c and d, together with the total transition rates $A_{\text{tot},1} = A_{\gamma,1} + A_{\text{A},1} = \Gamma_1/\hbar$ and likewise $A_{\text{tot},2}$ obtained by our own linewidth measurements for Li-like ions and from Ref. [25], form a set of four independent parameters, allowing one to calculate the four transition rates from them.

In Li-like ions, the calculated Auger rate of the line q is three orders of magnitude smaller than the radiative rate, and we did not measure any photoionization signal for this transition. Thus we set $A_{\text{A},q} = 0$ when comparing r or t with q, so the parameter c vanishes independently of the ion yield of r,t. This allows one to extract the transition rates of r and t just from fluorescence measurements, where the statistics are much better than for the photoion measurement. Due to the fully polarized photon beam, the angular distribution of the line q, which is a $J = 3/2 \rightarrow J = 1/2$ transition, is nonisotropic. Thus its apparent strength, when detected under 90°, is 1.25 times stronger. Furthermore, the linearly polarized light can only excite the $m = \pm\frac{1}{2}$ sublevels, so the degeneracy of the excited level is $g_q = 2$ instead of the usual $g = 2J + 1$. We calculated the rates using fluorescence and ion yields from r and t, and by using only fluorescence data of the lines r, q, and t. Apart from the total rates A_{tot} of r and t, these methods are independent from each other, so we further reduced uncertainties by combining both methods.

TABLE II. Radiative branching ratios for transitions from the excited states to states with different total angular momentum J. All values are given in percent. "Expt." denotes the value measured in this experiment, while the values under "Theory" are based on calculations from Palmeri *et al.* [17].

	$E1$		$E2$		$C1$		$C2$	
J	Expt.	Theory	Expt.	Theory	Expt.	Theory	Expt.	Theory
0	96.0(0.5)	96.5	85.9(2.8)	86.2	81.4(1.8)	74.8	5.9(3.8)	2.6
1	1.6(1.0)	0.1	5.4(3.4)	5.1	5.3(4.0)	1.7	71.3(8.5)	61.7
2	2.4(1.4)	3.4	8.8(5.1)	8.7	13.3(5.7)	23.5	22.8(12)	35.7

As depicted in Fig. 2, in the Be- and C-like ions the excited states do not only decay back to the ground state, but also have non-negligible transition rates to some metastable states. The resolution of our germanium detectors is too low to distinguish between these channels. Branching ratios between the ground state and metastable states differ for each transition. This affects our calculations in two ways. First, as the signal strength is only proportional to the excitation rate, we have to take into account the ground-state branching ratio $B = \frac{A_{\text{ground}}}{A_\gamma}$ when calculating d:

$$d = \frac{B_2}{B_1} d_{\text{measured}}. \tag{6}$$

Second, these metastable states have different angular momenta ($J = 0,1,2$). Hence, the angular distribution of the fluorescence photons is also different, as we excite with a fully polarized photon beam. As our detectors just cover a small solid angle, this changes their detection efficiency. However, the angular distribution of the decay channels can be calculated within the electric-dipole approximation for the electron-photon interaction [41], solely depending on the final angular momentum. We use this to determine the branching ratios between states with different J, by comparing the ratios of the 0°, 45°, and 90° detectors for these transitions. To calibrate solid-angle differences between the detectors, we use the isotropic distribution of the Li-like transitions r and t. The thus obtained radiative branching ratios are shown in Table II. We used them to correct for the different detection efficiencies when calculating the parameter c. Furthermore, for the transitions $E1$, $C1$, and $C2$ the ground state is the only state with $J = 0$ in which the excited states decay, therefore we also obtain their respective branching ratio B. Unfortunately, the excited state of the $E2$ transition can decay to two states with $J = 0$. Thus we cannot separate them in our experiment, so we rely on the calculated values of 77.1% to the $^1S_0$ ground state and 9.1% in the $^3P_0$ metastable state [17].

IV. RESULTS AND DISCUSSION

The resulting radiative and Auger rates of the measured transitions are listed in Table III. For the Li-like transitions the pure fluorescence data method is much more precise, giving a ≈10% uncertainty for the radiative rates. In general, the ion-fluorescence branching ratio (parameter c) yields a larger error, because, due to limited measurement time, the photoion statistics are rather poor. The large errors in the C-like transitions mostly derive from uncertainties in the $C2$ transition. Its total linewidth was measured to 385(207) meV [25] and the small branching ratio for decay to the ground state could only be determined to 5.9(3.8)% (see Table II), which leads to large errors for both the $C1$ and $C2$ transitions. Except for the parameter c, all other parameters can be measured without the need for photoion detection. Thus, these results may be improved by future pure resonant fluorescence spectroscopy measurements. Uncertainties due to the different decay channels for Be- and C-like ions could be reduced significantly by observing the fluorescence with a crystal spectrometer or a microcalorimeter, which would allow one to resolve the different channels. The data-taking duration of the measurement was only 4.5 h for the Li-like, 2.5 h for the Be-like, and 8.5 h for the C-like system, so the overall accuracy could be easily further improved by longer measurement times, as the current uncertainties arise mostly from statistics.

In Table IV our experimental results are compared with several theoretical calculations. Our values generally agree with theory, though the uncertainties are too large to distinguish between different theories, which also have estimated uncertainties of 10%–25%. However, it is noteworthy that all measured radiative rates tend to be slightly smaller

TABLE III. Radiative and Auger rates of x-ray excited states in Li-, Be-, and C-like iron, and corresponding 1-σ uncertainties. The total error consists of uncertainties in the linewidths (LW), the measured line strength ratios (LS), the measured ion-fluorescence branching ratio (BR), and the uncertainty in the branching ratio of the fluorescence decay channels (DC). In Li-like transitions only the combined contribution of LS and BR can be given (*). The total uncertainty is also listed as a percentage of the measured rate. All absolute values are in 10^{12} s^{-1}.

		Total error		Error composition			
Transition	Rate	Abs.	Rel.	LW	LS	BR	DC
r rad.	246.1	18.2	7%	18.1	2.2*	*	
r Auger	86.6	27.3	32%	27.2	2.5*	*	
t rad.	142.8	15.2	11%	15.1	1.6*	*	
t Auger	118.5	39.5	33%	39.5	1.8*	*	
q rad.	480.1	31.9	7%	31.9			
$E1$ rad.	440.6	88.1	20%	19.7	9.1	84.5	12.0
$E1$ Auger	223.3	86.6	39%	15.0	9.1	84.0	12.0
$E2$ rad.	42.5	9.1	21%	3.2	2.2	7.8	2.8
$E2$ Auger	235.5	50.1	21%	48.6	3.1	11.1	4.1
$C1$ rad.	273.5	171.7	63%	72.0	61.6	76.7	120.9
$C1$ Auger	531.7	173.2	33%	72.7	62.1	77.4	121.9
$C2$ rad.	577.3	255.2	44%	167.4	37.7	141.2	125.5
$C2$ Auger	325.1	220.3	68%	4.8	43.0	161.4	143.5

TABLE IV. Comparison of measured rates with theory. Theoretical values are obtained from calculations using AUTOSTRUCTURE [17], multiconfiguration Dirac-Fock (MCDF) [25], the MZ code [20](a), and the AUTOLSJ code [20](b).

	Radiative rate (10^{13} s^{-1})					Auger rate (10^{13} s^{-1})				
		Theory					Theory			
Line	This experiment	[17]	[25]	[20](a)	[20](b)	This experiment	[17]	[25]	[20](a)	[20](b)
r	24.6(1.8)	30.1	31.6	31.9	28.9	8.7(2.7)	4.2	4.9	3.2	3.8
t	14.3(1.5)	18.6	17.0	17.9	20.3	11.9(4.0)	6.8	7.9	9.0	7.4
q	48.0(3.2)	47.1	47.4	48.7			0.01	0.01	0.03	
$E1$	44.1(8.8)	45.3	44.4	45.5	45.3	22.3(8.7)	12.8	14.4	8.6	13.3
$E2$	4.3(0.9)	4.1	4.7	4.5	4.2	23.5(5.0)	18.6	20.7	14.7	17.5
$C1$	27.3(17.2)	36.3	33.1	35.2	32.1	53.2(17.3)	39.5	50.7	51.9	38.4
$C2$	57.7(25.5)	68.8	62.6	68.5	60.8	32.5(22.0)	24.1	20.5	32.4	25.6

than the theoretical values, while all the Auger rates are larger.

V. SUMMARY

In this experiment, radiative and Auger decay rates of K-shell-vacancy states of highly charged iron have been simultaneously measured, benchmarking theoretical calculations. Because of the lack of experimental data, these calculated data are exclusively used in spectral models such as *XSTAR* [42] and *Cloudy* [43]. Although the measured transitions are not yet resolved in celestial sources, this may change with the launch of the X-ray Calorimeter Spectrometer [44] on *ASTRO-H* [45] in 2015. It will be able to resolve the $K\alpha$ lines, thus providing rich information about x-ray binary stars and active galactic nuclei, as most of their properties can be derived from x-ray absorption and emittance of their accretion disks. Furthermore, our method can be easily transferred to other charge states and elements, e.g., for testing the claimed nonmonotonic Z dependence of transition rates in C-like ions [46].

ACKNOWLEDGMENTS

We thank A. Surzhykov for fruitful discussions regarding the alignment of the excited ions. The research leading to these results was supported by Deutsche Forschungsgemeinschaft (DFG). J.K.R. and C.B. received funding from DESY, a member of the Helmholtz Association (HGF).

[1] A. C. Fabian, K. Nandra, C. S. Reynolds, W. N. Brandt, C. Otani, Y. Tanaka, H. Inoue, and K. Iwasawa, On broad iron Kα lines in Seyfert 1 galaxies, Mon. Not. R. Astron. Soc. **277**, L11 (1995).

[2] J. M. Miller, A. C. Fabian, R. Wijnands, R. A. Remillard, P. Wojdowski, N. S. Schulz, T. Di Matteo, H. L. Marshall, C. R. Canizares, D. Pooley *et al.*, Resolving the composite Fe Kα emission line in the galactic black hole Cygnus X-1 with Chandra, Astrophys. J. **578**, 348 (2002).

[3] J. M. Miller, J. Raymond, C. S. Reynolds, A. C. Fabian, T. R. Kallman, and J. Homan, The accretion disk wind in the black hole GRO J1655-40, Astrophys. J. **680**, 1359 (2008).

[4] G. Matt, W. N. Brandt, and A. C. Fabian, The iron Kα line complex in Compton-thick Seyfert 2 galaxies, Mon. Not. R. Astron. Soc. **280**, 823 (1996).

[5] K. Nandra, On the origin of the iron Kα line cores in active galactic nuclei, Mon. Not. R. Astron. Soc. **368**, L62 (2006).

[6] T. Yaqoob, I. M. George, K. Nandra, T. J. Turner, P. J. Serlemitsos, and R. F. Mushotzky, Physical diagnostics from a narrow Fe Kα emission line detected by Chandra in the Seyfert 1 galaxy NGC 5548, Astrophys. J. **546**, 759 (2001).

[7] J. C. Lee, K. Iwasawa, J. C. Houck, A. C. Fabian, H. L. Marshall, and C. R. Canizares, The shape of the relativistic iron Kα line from MCG-6-30-15 measured with the Chandra high energy transmission grating spectrometer and the Rossi x-ray timing explorer, Astrophys. J. Lett. **570**, L47 (2002).

[8] M. Eracleous, J. P. Halpern, and M. Livio, The resolved Fe K alpha line of the broad-line radio galaxy 3C 390.3 and its implications, Astrophys. J. **459**, 89 (1996).

[9] P. Lubinski and A. A. Zdziarski, The strength and width of Fe Kα lines in Seyferts and their correlations with the x-ray slope, Mon. Not. R. Astron. Soc. **323**, L37 (2001).

[10] T. Kallman, D. A. Evans, H. Marshall, C. Canizares, A. Longinotti, M. Nowak, and N. Schulz, A census of x-ray gas in NGC 1068: Results from 450 ks of Chandra high energy transmission grating observations, Astrophys. J. **780**, 121 (2014).

[11] M. D. Trigo, J. C. A. Miller-Jones, S. Migliari, J. W. Broderick, and T. Tzioumis, Baryons in the relativistic jets of the stellar-mass black-hole candidate 4U 1630-47, Nature (London) **504**, 260 (2013).

[12] G. Matt, S. Bianchi, M. Guainazzi, and S. Molendi, The high energy emission line spectrum of NGC 1068, Astron. Astrophys. **414**, 155 (2004).

[13] N. S. Schulz, T. E. Kallman, D. K. Galloway, and W. N. Brandt, The variable warm absorber in Circinus X-1, Astrophys. J. **672**, 1091 (2008).

[14] M. T. Reynolds and J. M. Miller, Chandra grating spectroscopy of the Be/x-ray binary 1A 0535+262, Astrophys. J. **723**, 1799 (2010).

[15] J. F. Seely, U. Feldman, and U. I. Safronova, Measurement of wavelengths and lamb shifts for inner-shell transitions in Fe XVIII-XXIV, Astrophys. J. **304**, 838 (1986).

[16] S. N. Nahar, A. K. Pradhan, and H. L. Zhang, *K*-shell dielectronic resonances in photoabsorption: Differential oscillator strengths for Li-like C IV, O VI, and Fe XXIV, Phys. Rev. A **63**, 060701 (2001).

[17] P. Palmeri, C. Mendoza, T. R. Kallman, and M. A. Bautista, A complete set of radiative and Auger rates for K-vacancy states in Fe XVIII-Fe XXV, Astron. Astrophys. **403**, 1175 (2003).

[18] M. H. Chen, Relativistic Auger and x-ray emission rates of the $1s2l^n$ $(2l')^m$ configurations of Be-like ions, Phys. Rev. A **31**, 1449 (1985).

[19] M. Cornille, J. Dubau, M. Loulergue, F. Bely-Dubau, P. Faucher, U. I. Safronova, A. S. Shlyaptseva, and L. Vainshtein, Fe XXIII-Fe XIX theoretical spectra in two calculational methods, J. Phys. B: At. Mol. Opt. Phys. **21**, 3347 (1988).

[20] T. Kato, U. I. Safronova, A. S. Shlyaptseva, M. Cornille, J. Dubau, and J. Nilsen, Comparison of satellite spectra for H-like Fe and He-like Fe, Ca, and S calculated by three different methods, At. Data Nucl. Data Tables **67**, 225 (1997).

[21] M. Bitter, K. W. Hill, N. R. Sauthoff, P. C. Efthimion, E. Meservey, W. Roney, S. von Goeler, R. Horton, M. Goldman, and W. Stodiek, Dielectronic satellite spectrum of heliumlike iron (Fe XXV), Phys. Rev. Lett. **43**, 129 (1979).

[22] P. Beiersdorfer, T. Phillips, V. L. Jacobs, K. W. Hill, M. Bitter, S. von Goeler, and S. M. Kahn, High-resolution measurements, line identification, and spectral modeling of K-alpha transitions in Fe-XVIII-Fe-XXV, Astrophys. J. **409**, 846 (1993).

[23] V. Decaux, P. Beiersdorfer, S. M. Kahn, and V. L. Jacobs, High resolution measurements of the Kα spectrum of Fe XXV–XVIII: New spectral diagnostics of nonequilibrium astrophysical plasmas, Astrophys. J. **482**, 1076 (1997).

[24] P. Beiersdorfer, T. W. Phillips, K. L. Wong, R. E. Marrs, and D. A. Vogel, Measurement of level-specific dielectronic-recombination cross-sections of heliumlike Fe-XXV, Phys. Rev. A **46**, 3812 (1992).

[25] J. K. Rudolph, S. Bernitt, S. W. Epp, R. Steinbrügge, C. Beilmann, G. V. Brown, S. Eberle, A. Graf, Z. Harman, N. Hell *et al.*, X-ray resonant photoexcitation: Linewidths and energies of $K\alpha$ transitions in highly charged Fe ions, Phys. Rev. Lett. **111**, 103002 (2013).

[26] H. Kjeldsen, Photoionization cross sections of atomic ions from merged-beam experiments, J. Phys. B: At. Mol. Opt. Phys. **39**, R325 (2006).

[27] M. C. Simon, M. Schwarz, S. W. Epp, C. Beilmann, B. L. Schmitt, Z. Harman, T. M. Baumann, P. H. Mokler, S. Bernitt, R. Ginzel *et al.*, Photoionization of N^{3+} and Ar^{8+} in an electron beam ion trap by synchrotron radiation, J. Phys. B: At. Mol. Opt. Phys. **43**, 065003 (2010).

[28] M. C. Simon, J. R. Crespo López-Urrutia, C. Beilmann, M. Schwarz, Z. Harman, S. W. Epp, B. L. Schmitt, T. M. Baumann, E. Behar, S. Bernitt *et al.*, Resonant and near-threshold photoionization cross sections of Fe^{14+}, Phys. Rev. Lett. **105**, 183001 (2010).

[29] S. W. Epp, J. R. Crespo López-Urrutia, G. Brenner, V. Mäckel, P. H. Mokler, R. Treusch, M. Kuhlmann, M. V. Yurkov, J. Feldhaus, J. R. Schneider *et al.*, Soft x-ray laser spectroscopy on trapped highly charged ions at FLASH, Phys. Rev. Lett. **98**, 183001 (2007).

[30] S. W. Epp, J. R. Crespo López-Urrutia, M. C. Simon, T. Baumann, G. Brenner, R. Ginzel, N. Guerassimova, V. Mäckel, P. H. Mokler, B. L. Schmitt *et al.*, X-ray laser spectroscopy of highly charged ions at FLASH, J. Phys. B: At. Mol. Opt. Phys. **43**, 194008 (2010).

[31] S. Bernitt, G. V. Brown, J. K. Rudolph, R. Steinbrügge, A. Graf, M. Leutenegger, S. W. Epp, S. Eberle, K. Kubiček, V. Mäckel *et al.*, An unexpectedly low oscillator strength as the origin of the Fe XVII emission problem, Nature (London) **492**, 225 (2012).

[32] S. W. J. Scully, I. Álvarez, C. Cisneros, E. D. Emmons, M. F. Gharaibeh, D. Leitner, M. S. Lubell, A. Müller, R. A. Phaneuf, R. Püttner *et al.*, Doubly excited resonances in the photoionization spectrum of Li^+: Experiment and theory, J. Phys. B: At. Mol. Opt. Phys. **39**, 3957 (2006).

[33] A. Müller, S. Schippers, R. A. Phaneuf, S. W. J. Scully, A. Aguilar, C. Cisneros, M. F. Gharaibeh, A. S. Schlachter, and B. M. McLaughlin, *K*-shell photoionization of Be-like boron (B^+) ions: Experiment and theory, J. Phys. B: At. Mol. Opt. Phys. **47**, 135201 (2014).

[34] A. Müller, S. Schippers, R. A. Phaneuf, S. W. J. Scully, A. Aguilar, C. Cisneros, M. F. Gharaibeh, A. S. Schlachter, and B. M. McLaughlin, K-shell photoionization of ground-state Li-like boron ions [B^{2+}]: Experiment and theory, J. Phys. B: At. Mol. Opt. Phys. **43**, 135602 (2010).

[35] S. W. J. Scully, A. Aguilar, E. D. Emmons, R. A. Phaneuf, M. Halka, D. Leitner, J. C. Levin, M. S. Lubell, R. Püttner, A. S. Schlachter *et al.*, K-shell photoionization of Be-like carbon ions: Experiment and theory for C^{2+}, J. Phys. B: At. Mol. Opt. Phys. **38**, 1967 (2005).

[36] A. Müller, S. Schippers, R. A. Phaneuf, S. W. J. Scully, A. Aguilar, A. M. Covington, I. Álvarez, C. Cisneros, E. D. Emmons, M. F. Gharaibeh *et al.*, K-shell photoionization of ground-state Li-like carbon ions [C^{3+}]: Experiment, theory and comparison with time-reversed photorecombination, J. Phys. B: At. Mol. Opt. Phys. **42**, 235602 (2009).

[37] M. F. Gharaibeh, J. M. Bizau, D. Cubaynes, S. Guilbaud, N. E. Hassan, M. M. A. Shorman, C. Miron, C. Nicolas, E. Robert, C. Blancard *et al.*, K-shell photoionization of singly ionized atomic nitrogen: Experiment and theory, J. Phys. B: At. Mol. Opt. Phys. **44**, 175208 (2011).

[38] M. F. Gharaibeh, N. E. Hassan, M. M. A. Shorman, J. M. Bizau, D. Cubaynes, S. Guilbaud, I. Sakho, C. Blancard, and B. M. McLaughlin, K-shell photoionization of B-like atomic nitrogen ions: Experiment and theory, J. Phys. B: At. Mol. Opt. Phys. **47**, 065201 (2014).

[39] M. M. A. Shorman, M. F. Gharaibeh, J. M. Bizau, D. Cubaynes, S. Guilbaud, N. E. Hassan, C. Miron, C. Nicolas, E. Robert, I. Sakho *et al.*, *K*-shell photoionization of Be-like and Li-like ions of atomic nitrogen: Experiment and theory, J. Phys. B: At. Mol. Opt. Phys. **46**, 195701 (2013).

[40] H.-C. Wille, H. Franz, R. Röhlsberger, W. A. Caliebe, and F.-U. Dill, Nuclear resonant scattering at PETRA III: Brillant opportunities for nano — and extreme condition science, J. Phys.: Conf. Ser. **217**, 012008 (2010).

[41] V. V. Balashov, A. N. Grum-Grzhimailo, and N. M. Kabachnik, *Polarization and Correlation Phenomena in Atomic Collisions: A Practical Theory Course* (Springer Science+Business Media, New York, 2000).

[42] M. A. Bautista and T. R. Kallman, The XSTAR atomic database, Astrophys. J. Suppl. **134**, 139 (2001).

[43] G. J. Ferland, R. L. Porter, P. A. M. van Hoof, R. J. R. Williams, N. P. Abel, M. L. Lykins, G. Shaw, W. J. Henney, and P. C. Stancil, The 2013 release of cloudy, Rev. Mex. Astron. Astrofis. **49**, 137 (2013).

[44] K. Mitsuda, R. L. Kelley, K. R. Boyce, G. V. Brown, E. Costantini, M. J. DiPirro, Y. Ezoe, R. Fujimoto, K. C. Gendreau, J.-W. den Herder *et al.*, The high-resolution x-ray microcalorimeter spectrometer system for the SXS on ASTRO-H, Proc. SPIE **7732**, 773211 (2010).

[45] T. Takahashi, K. Mitsuda, R. Kelley, H. Aarts, F. Aharonian, H. Akamatsu, F. Akimoto, S. Allen, N. Anabuki, L. Angelini *et al.*, The ASTRO-H x-ray observatory, Proc. SPIE **8443**, 84431Z (2012).

[46] M. F. Hasoğlu, D. Nikolić, T. W. Gorczyca, S. T. Manson, M. H. Chen, and N. R. Badnell, Nonmonotonic behavior as a function of nuclear charge of the *K*-shell Auger and radiative rates and fluorescence yields along the $1s2s^22p^3$ isoelectronic sequence, Phys. Rev. A **78**, 032509 (2008).